



OPEN

DATA DESCRIPTOR

Molecular dynamics trajectories for 630 coarse-grained drug-membrane permeations

Christian Hoffmann¹, Alessia Centi¹, Roberto Menichetti^{1,2,3} & Tristan Berau¹✉

The permeation of small-molecule drugs across a phospholipid membrane bears much interest both in the pharmaceutical sciences and in physical chemistry. Connecting the chemistry of the drug and the lipids to the resulting thermodynamic properties remains of immediate importance. Here we report molecular dynamics (MD) simulation trajectories using the coarse-grained (CG) Martini force field. A wide, representative coverage of chemistry is provided: across solutes—exhaustively enumerating all 105 CG dimers—and across six phospholipids. For each combination, umbrella-sampling simulations provide detailed structural information of the solute at all depths from the bilayer midplane to bulk water, allowing a precise reconstruction of the potential of mean force. Overall, the present database contains trajectories from 15,120 MD simulations. This database may serve the further identification of structure-property relationships between compound chemistry and drug permeability.

Background & Summary

The passive permeation of small organic, drug-like molecules across phospholipid membranes has garnered much interest, not only to practically optimize pharmaceutical properties, but also as a more fundamental physical-chemistry problem¹. The latter acts as a testbed to understand the molecular driving forces at play during a permeation process across a soft interface. A more robust understanding of the structure-property relationship can be obtained by screening across chemistries and systematically measuring the permeability coefficient from *in vitro* experiments^{2,3}. Given the small size and apparent bias of databases of experimental compounds⁴, the perspective to harness computational methods at high throughput has been on the rise^{5–9}.

Permeation is described using the inhomogeneous solubility-diffusion model to yield a diffusion process in terms of a one-dimensional Smoluchowski equation along z —the normal to the membrane midplane. The resulting permeability coefficient, P , takes the form

$$P^{-1} = \int dz \frac{\exp[\beta G(z)]}{D(z)}, \quad (1)$$

where $\beta^{-1} = k_B T$ is the inverse temperature, $G(z)$ is the potential of mean force (PMF), and $D(z)$ is the local diffusivity. As such, knowledge of $G(z)$ and $D(z)$ enables an *in silico* estimation of P , which may be obtained from molecular dynamics (MD) simulations. While the direct estimation of these quantities from brute-force MD typically fails, enhanced-sampling methods have provided a robust strategy to estimate both $G(z)$ and $D(z)$. Equation 1 depends exponentially on $G(z)$, but only linearly on $D(z)$, making the latter quantity less critical—it was also found to depend rather weakly on the chemistry of the drug¹⁰. A large number of enhanced-sampling studies have demonstrated the capability to not only converge the PMF, but also to provide permeability coefficients that exhibit high correlation with experimental measurements^{10–16}. An illustrative example of the PMF is shown in Fig. 1a, together with a cartoon of a phospholipid membrane in the background.

The *in silico* route is predictive and generalizable in that it does not rely on adjustable parameters: the main input of an MD simulation is the force field, often parametrized on properties unrelated to interactions with a phospholipid membrane^{17,18}. Critically, this limits the danger of overfitting observed in statistical models¹⁹. The main downside of using MD simulations is the computational investment: atomistic simulations with explicit

¹Max Planck Institute for Polymer Research, 55128, Mainz, Germany. ²Physics Department, University of Trento, 38123, Trento, Italy. ³INFN-TIFPA, Trento Institute for Fundamental Physics and Applications, 38123, Trento, Italy. ✉e-mail: berau@mpip-mainz.mpg.de

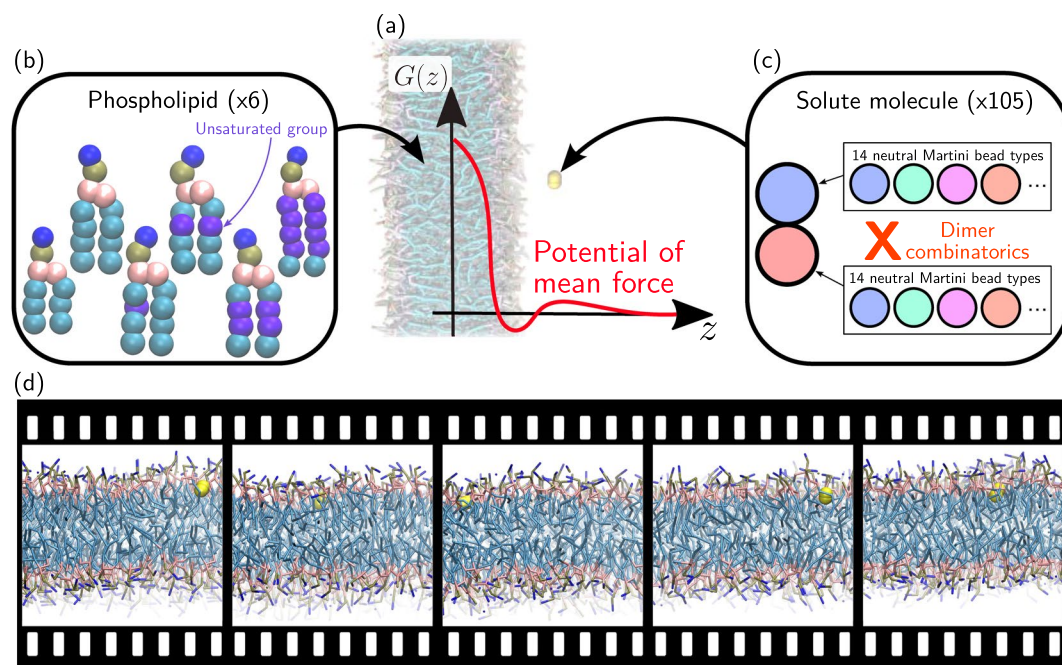


Fig. 1 Drug-membrane computer simulation setup; screening over both phospholipids and solute molecules. **(a)** Background: Simulation setup of a solute (yellow) partitioning between water (not shown) and the lipid membrane. Foreground: Potential of mean force along the normal of the bilayer, $G(z)$. **(b)** Lipid membrane: Cartoon representations of the five phospholipids, differing in the number of unsaturated groups. **(c)** Solute molecule: Combinatorics of all 105 CG Martini dimers. **(d)** The present dataset contains the trajectory of each MD simulation.

Polarity	Type	HB	$\Delta G_{\text{ol} \rightarrow \text{w}}$
hydrophilic	P5	—	−2.1
	P4	—	−2.2
	P3	—	−2.1
	P2	—	−0.9
	P1	—	−0.5
neutral	Nda	d, a	0.6
	Nd	d	0.6
	Na	a	0.6
	N0	—	1.0
hydrophobic	C5	—	1.7
	C4	—	2.4
	C3	—	3.0
	C2	—	3.3
	C1	—	3.4

Table 1. Characteristics of non-charged Martini bead types. The table contains information about the bead-type name (Type), hydrogen-bonding capability (HB, “d” and “a” for donor and acceptor, respectively), and the octanol/water partitioning free energy ($\Delta G_{\text{ol} \rightarrow \text{w}} = \Delta G_{\text{water}} - \Delta G_{\text{octanol}}$, in units of kcal/mol), as reported elsewhere³⁸.

solvent typically require 10^5 CPU-hours for a small molecule in a single-component lipid membrane^{10,13,14,20}, hindering the prospects of running them at high-throughput.

We have recently proposed the use of coarse-grained (CG) models to tackle this problem. Coarse-graining can enable a more efficient sampling of the conformational space by lumping together atoms into super-particles or beads^{21,22}. In particular we relied on the CG Martini model^{23–25}, which is specifically tailored to reproduce the partitioning behavior of compounds in different environments—thus making it particularly well suited for permeability calculations. The modularity of Martini means that it constructs molecules based on a small set of bead types, each one encoding different chemical properties—mainly hydrophobicity, hydrogen-bonding, and charge (see Table 1 for details). We reported the systematic calculation of PMFs using umbrella sampling for all

Membrane	N_L	N_W	N_{AF}
DAPC	128	2430	270
DIPC	128	2120	236
DLPC	128	1883	209
DOPC	128	1890	189
DPPC	128	2014	224
POPC	128	2014	224

Table 2. Composition of single-lipid bilayer membranes. N_L = number of lipid molecules, N_W = number of water beads, N_{AF} = number of anti-freeze beads. DAPC = 1,2-diarachidonoyl-*sn*-glycero-3-phosphocholine. DIPC = 1,2-dilinoleoyl-*sn*-glycero-3-phosphocholine. DLPC = 1,2-dilauroyl-*sn*-glycero-3-phosphocholine. DOPC = 1,2-dioleoyl-*sn*-glycero-3-phosphocholine. DPPC = 1,2-dipalmitoyl-*sn*-glycero-3-phosphocholine. POPC = 1-palmitoyl-2-oleoyl-*sn*-glycero-3-phosphocholine.

Folder/File	I/O	Description
us-x/		
equ.cpt	I	binary; checkpoint to extend a previous simulation
equ.gro	I	coordinates of the starting configuration
system.top	I	topology of the molecular system
martini_v2.2.itp	I	Force field and parameters
martini_v2.0_lipids.itp	I	Lipid force field
mol3.itp,mol3-2.itp	I	Solute force field
prod.mdp	I	simulation parameters
prod.tpr	I	binary; overall simulation information
prod.xtc	O	binary; trajectory
prod.edr	O	binary; various observables (e.g., energies)
prodx-umbrella0.xvg	O	time evolution of the solute CoMs along the z axis
prodf-umbrella0.xvg	O	time evolution of the pull forces along the z axis
pmf/		
tpr-files.dat	I	indexes paths to the tpr files
pullx-files.dat	I	indexes paths to the prodx files
bsResult.xvg	O	PMF profile with error bars

Table 3. Supplied files and their purpose. All files provided in text format unless specified otherwise. I/O = input/output. CoM = center of mass.

CG compounds made of one and two neutral beads (hereafter denoted unimers and dimers)²⁶. This amounted to 14 unimers and $14 \times 15/2 = 105$ dimers (Fig. 1c). The thermodynamic parametrization of Martini yields accurate PMFs, as compared to reference curves from atomistic simulations, as well as remarkably-accurate permeability coefficients, as compared to reference simulations and experiments²⁷. Because of the transferable nature of Martini, the CG model significantly reduces the size of chemical space, such that these 119 computer simulations offer estimates for more than 500,000 small molecules^{26,27}. We more recently extended our approach to linear trimers and tetramers, demonstrating that the screening range can be significantly increased²⁸. As such, Martini offers a robust methodology to run high-throughput computer simulations of drug-membrane permeability.

The present database reports the full umbrella-sampling MD trajectories necessary to run PMF calculations for all Martini dimers in six different single-component phospholipid membranes. The 105 dimers inserted in 6 membranes amounts to 630 drug-membrane combinations (Fig. 1). Given that each PMF calculation relied on 24 umbrella sampling simulations, the present database contains 15,120 MD trajectories. The diversity of compound and lipid chemistries can offer unprecedented insight into the underlying thermodynamics^{26,29}. Below we present an example use of the present database by displaying the tilt angle of each compound across membrane-insertion depth and compound chemistry. We believe that the raw MD trajectories provided for this breadth of chemistries will provide further insight into the structure-property relationships governing drug-membrane permeability.

Methods

We follow previously established simulation protocols that are described in detail elsewhere²⁶. In brief, we built symmetric, single-lipid bilayer membranes that contain 64 lipids per leaflet using the INSANE script³⁰. Table 2 informs on the composition of the various membrane systems that differ in the number of water beads. As it is common practice, we replaced at least 10% of the non-polarizable Martini waters by anti-freeze beads. Simulations were performed in GROMACS 4.6.6³¹ using the Martini force field with standard input parameters³². We ran simulations in the *NPT* ensemble at 300 K and 1 bar controlled by means of a stochastic velocity-rescaling thermostat³³ and a Parrinello-Rahman barostat³⁴, respectively. We performed umbrella sampling along the bilayer normal (*z*-axis) in a range from 0.0 to 4.1 nm at a step size of 0.1 nm by generating 24 windows in which the

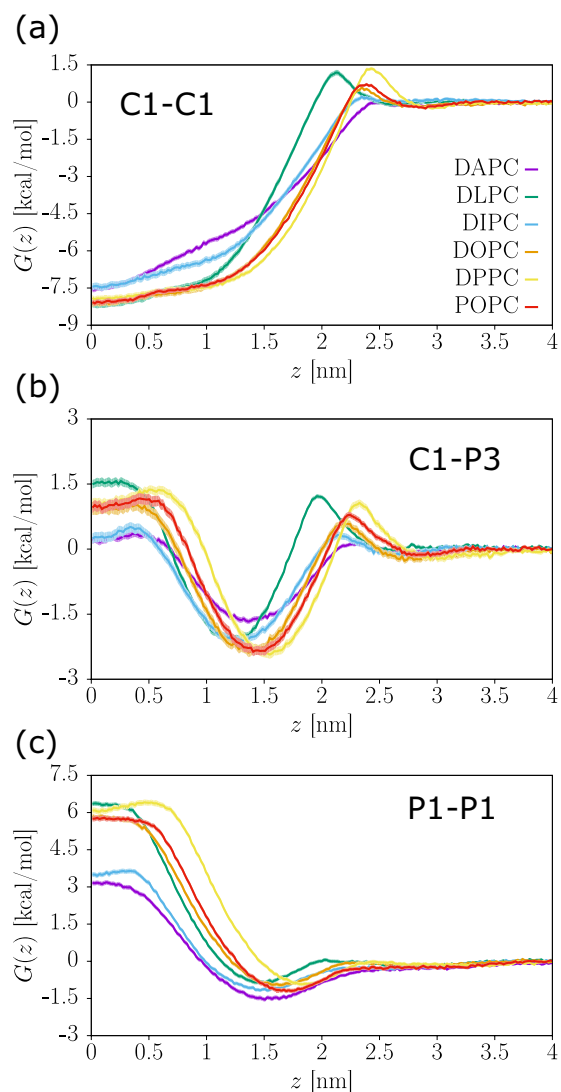


Fig. 2 Examples of PMF profiles in different lipid environments. Three representative solutes are shown: (a) hydrophobic (C1-C1); (b) amphiphilic (C1-P3); and (c) polar (P1-P1). See labels for the different lipid types.

solute is centered via a harmonic biasing potential ($k = 240$ kcal/mol/nm²). For computational efficiency, each simulation box contained two solute compounds placed in different membrane leaflets. Each window included a sequence of minimization, heat-up, and equilibration runs prior to the production one, the latter being simulated for $1.2 \cdot 10^5 \tau$ using a time step of $\delta t = 0.02 \tau$, where τ (1 ps) refers to the model's natural unit of time. PMF profiles were then reconstructed by means of the weighted histogram analysis method (WHAM)^{35,36}, with error bars estimated from 100 bootstraps.

Data Records

We provide datasets for MD trajectories of solute-membrane systems at a CG resolution for 105 solutes inserted in six different phospholipid bilayers³⁷. Each dataset is denoted by the abbreviated name of the lipid and deposited as a single archive file, e.g., DPPC.tar.bz2. Within a dataset, there are 105 folders containing the trajectories and PMF profile of a particular solute, following the naming convention DIM_bead1-bead2, where bead1 and bead2 denote the relevant bead types following the standard Martini notation (see Table 1). For improved sampling we have systematically placed *two* solutes in each simulation box, always separated by a normal distance (i.e., only along z) of 4.1 nm. The trajectories obtained from umbrella sampling (US) are stored in sub-folders denoted us-x, where x takes values 0.0, 0.1, ..., 2.4, corresponding to the reference depth in the bilayer of one of the two solutes. For instance, the folder us-2.4 contains two solutes restrained around $z_1 = 2.4$ nm and $z_2 = -1.7$ nm. The US sub-folders contain all necessary input files to repeat the production runs as well as the respective output files, including trajectories and observables. The sub-folder pmf contains the input files to perform WHAM reweighting in GROMACS and the output PMF profiles. Table 3 lists all files included in the sub-folders us-x and pmf together with a brief description of their purpose. In Fig. 2 we report typical PMF

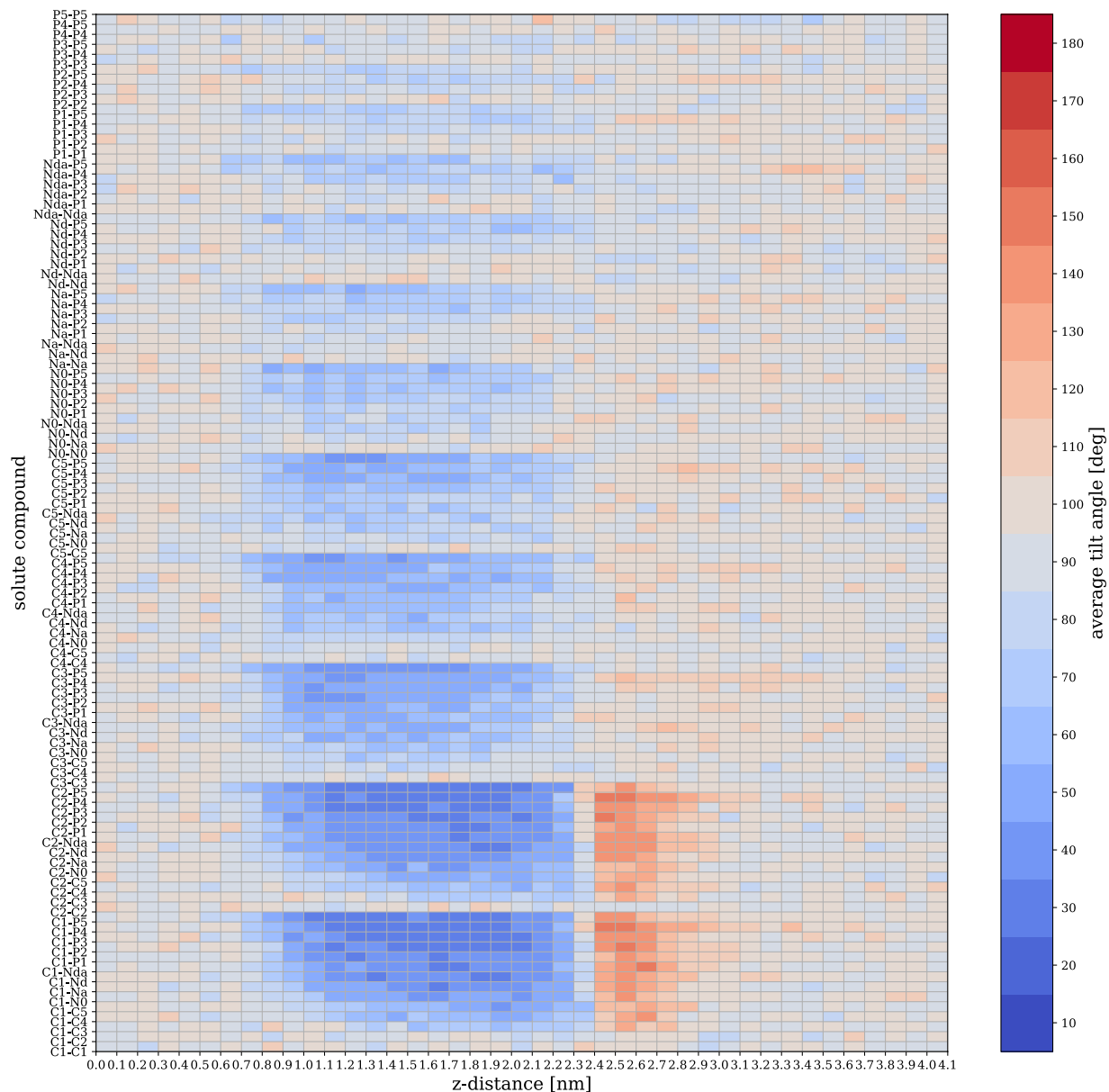


Fig. 3 Average tilt angle in a DPPC bilayer as function of the z-distance across all 105 solute compounds.

profiles obtained for hydrophobic (Fig. 2a), amphiphilic (Fig. 2b), and polar solute compounds (Fig. 2c) across all considered lipid environments.

Our records indicate a computational investment to run heat-up, equilibration, and production simulations of roughly 0.5, 1, and 8 CPU-hours per umbrella, respectively. Summing up over all 15,120 MD simulations supplied, this amounts to roughly 150,000 CPU-hours to generate the present dataset.

Technical Validation

A number of studies using the same simulation protocol have demonstrated the thermodynamic validity and accuracy of CG Martini simulations. Bereau and Kremer found a mean absolute error between experimental and Martini transfer free energies between water and octanol of 0.79 kcal/mol across 653 neutral small organic molecules—an excellent result given the minimalism of the model³⁸. By further invoking relations between bulk transfer free energies, used as proxy for various environments of the membrane, we deduced a mean absolute error on features of our CG PMFs of approximately 1.4 kcal/mol²⁶. This remarkable agreement had been earlier probed specifically for amino acids³⁹. On a structural level, we showed that backmapping CG snapshots and running short atomistic MD simulations offered a significant speedup in convergence of the atomistic PMF calculations, suggesting that the conformational ensemble of the CG model adequately matches its atomistic counterpart⁴⁰. Moreover, as the permeability coefficient depends exponentially on the PMF, reliable estimates of the latter prove necessary¹³. We showed that the accuracy of the PMFs obtained through Martini translated into excellent predictability for the permeability coefficient—roughly 1 log unit^{27,29}.

Usage Notes

The 15,120 MD trajectories in this dataset provide a rich amount of information. As an illustration, we focus on the orientation of the solute with respect to the normal of the membrane bilayer. We define a tilt angle θ between the bond vector of the solute and the normal vector of the membrane, oriented as to point from the the bilayer midplane to the membrane surface. Figure 3 displays the average tilt angle as a function of the depth z in a DPPC bilayer across all 105 solute compounds. The depicted angles are normalized to $\sin \theta$ to account for the Jacobian of the transformation to spherical coordinates.

We find that solutes composed of two beads of identical or similar polarity display no preferred orientation, such that $\theta \approx 90^\circ$. On the other hand, features appear for compounds that show a *difference* in polarity between the two beads of the solute. These features are markedly present in the range of depths $0.9 < z < 2.2$ nm, which entails the lipid tail region. These amphiphilic solutes, such as C1-P5, show a strong preference for small tilt angles $\theta < 45^\circ$, where the more hydrophobic bead is facing the membrane core. The lack of features below $z \approx 0.9$ nm is likely due to the force field's interaction cut-off. In addition, strongly amphiphilic solutes also show orientational order at the membrane/water interface ($2.4 < z < 2.7$ nm), but with a flipped bond vector ($\theta \approx 130^\circ$), i.e., the polar site now faces the membrane.

Code availability

No custom code was used to generate this dataset. Simulations were run using GROMACS 4.6.6, and all input files used to generate the trajectories are contained in the present dataset. The output data contains a number of binary files, all generated from GROMACS. GROMACS is available across many platforms and architectures (see Gromacs manual) and its output files can be read either from a compiled version of the freely-available code, or from other analysis modules, such as MDANALYSIS⁴¹ or MDTRAJ⁴².

The WHAM-reconstructed PMFs were obtained by running a command that can be found in each DIM_bead1-bead2/pmf/bsResult.xvg file.

Received: 7 October 2019; Accepted: 22 January 2020;

Published online: 13 February 2020

References

- Stein, W. *Transport and diffusion across cell membranes*. (Elsevier, Amsterdam, 2012).
- Pidgeon, C. *et al.* Iam chromatography: an *in vitro* screen for predicting drug membrane permeability. *J. Med. Chem.* **38**, 590–594 (1995).
- Yazdani, M., Glynn, S. L., Wright, J. L. & Hawi, A. Correlating partitioning and caco-2 cell permeability of structurally diverse small molecular weight compounds. *Pharm. Res.* **15**, 1490–1494 (1998).
- Lin, A. *et al.* Mapping of the available chemical space versus the chemical universe of lead-like compounds. *Chem. Med. Chem.* **13**, 540–554 (2018).
- Pyzer-Knapp, E. O., Suh, C., Gómez-Bombarelli, R., Aguilera-Iparraguirre, J. & Aspuru-Guzik, A. What is high-throughput virtual screening? A perspective from organic materials discovery. *Annu. Rev. Mater. Res.* **45**, 195–216 (2015).
- Ghiringhelli, L. M., Vybiral, J., Levchenko, S. V., Draxl, C. & Scheffler, M. Big data of materials science: critical role of the descriptor. *Phys. Rev. Lett.* **114**, 105503 (2015).
- Bereau, T., Andrienko, D. & Kremer, K. Research Update: Computational materials discovery in soft matter. *APL Materials* **4**, 6391–6400 (2016).
- Faber, F. A., Lindmaa, A., Von Lilienfeld, O. A. & Armiento, R. Machine learning energies of 2 million elpasolite (ABC₂D₆) crystals. *Phys. Rev. Lett.* **117**, 135502 (2016).
- Ramprasad, R., Batra, R., Pilia, G., Mannodi-Kanakkithodi, A. & Kim, C. Machine learning in materials informatics: recent applications and prospects. *npj Comput. Mater.* **3**, 54 (2017).
- Carpenter, T. S. *et al.* A method to predict blood-brain barrier permeability of drug-like compounds using molecular dynamics simulations. *Biophys. J.* **107**, 630–641 (2014).
- Parisio, G., Stocchero, M. & Ferrarini, A. Passive membrane permeability: beyond the standard solubility-diffusion model. *J. Chem. Theory Comput.* **9**, 5236–5246 (2013).
- Votapka, L. W., Lee, C. T. & Amaro, R. E. Two relations to estimate membrane permeability using milestoning. *J. Phys. Chem. B* **120**, 8606–8616 (2016).
- Lee, C. T. *et al.* Simulation-based approaches for determining membrane permeability of small compounds. *J. Chem. Inf. Model.* **56**, 721–733 (2016).
- Bennion, B. J. *et al.* Predicting a drug's membrane permeability: A computational model validated with *in vitro* permeability assay data. *J. Phys. Chem. B* **121**, 5228–5237 (2017).
- De Vos, O. *et al.* Membrane permeability: Characteristic times and lengths for oxygen and a simulation-based test of the inhomogeneous solubility-diffusion model. *J. Chem. Theory Comput.* **14**, 3811–3824 (2018).
- Sun, R. *et al.* Molecular transport through membranes: Accurate permeability coefficients from multidimensional potentials of mean force and local diffusion constants. *J. Chem. Phys.* **149**, 072310 (2018).
- Vanommeslaeghe, K. & MacKerell, A. Jr. Charmm additive and polarizable force fields for biophysics and computer-aided drug design. *Biochim. Biophys. Acta* **1850**, 861–871 (2015).
- Wang, L.-P. *et al.* Building a more predictive protein force field: a systematic and reproducible route to amber-fb15. *J. Phys. Chem. B* **121**, 4023–4039 (2017).
- Swift, R. V. & Amaro, R. E. Back to the future: can physical models of passive membrane permeability help reduce drug candidate attrition and move us beyond QSPR? *Chem. Biol. Drug. Des.* **81**, 61–71 (2013).
- Tse, C. H., Comer, J., Wang, Y. & Chipot, C. The link between membrane composition and permeability to drugs. *J. Chem. Theory Comput.* (2018).
- Voth, G. A. *Coarse-graining of condensed phase and biomolecular systems*. (CRC press, Boca Raton, FL, 2008).
- Noid, W. G. Perspective: Coarse-grained models for biomolecular systems. *J. Chem. Phys.* **139**, 090901 (2013).
- Marrink, S. J., Risselada, H. J., Yefimov, S., Tieleman, D. P. & De Vries, A. H. The Martini force field: coarse grained model for biomolecular simulations. *J. Phys. Chem. B* **111**, 7812–7824 (2007).
- Periole, X. & Marrink, S.-J. The Martini coarse-grained force field. In *Biomolecular Simulations*, 533–565 (Springer, 2013).
- Marrink, S. J. & Tieleman, D. P. Perspective on the Martini model. *Chem. Soc. Rev.* **42**, 6801–6822 (2013).
- Menichetti, R., Kanekal, K. H., Kremer, K. & Bereau, T. In silico screening of drug-membrane thermodynamics reveals linear relations between bulk partitioning and the potential of mean force. *J. Chem. Phys.* **147**, 125101 (2017).

27. Menichetti, R., Kanekal, K. H. & Bereau, T. Drug–membrane permeability across chemical space. *ACS Centr. Sci.* **5**, 290–298 (2019).
28. Hoffmann, C., Menichetti, R., Kanekal, K. H. & Bereau, T. Controlled exploration of chemical space by machine learning of coarse-grained representations. *Phys. Rev. E* **100**, 033302 (2019).
29. Menichetti, R. & Bereau, T. Revisiting the Meyer-Overton rule for drug-membrane permeabilities. *Mol. Phys.* 1–10 (2019).
30. Wassenaar, T. A., Ingólfsson, H. I., Böckmann, R. A., Tieleman, D. P. & Marrink, S. J. Computational lipidomics with Insane: A versatile tool for generating custom membranes for molecular simulations. *J. Chem. Theory Comput.* **11**, 2144–2155 (2015).
31. Hess, B., Kutzner, C., van der Spoel, D. & Lindahl, E. GROMACS 4: Algorithms for highly efficient, load-balanced, and scalable molecular simulation. *J. Chem. Theory Comput.* **4**, 435–447 (2008).
32. de Jong, D. H., Baoukina, S., Ingólfsson, H. I. & Marrink, S. J. Martini straight: Boosting performance using a shorter cutoff and GPUs. *Comput. Phys. Comm.* **199**, 1–7 (2016).
33. Bussi, G., Donadio, D. & Parrinello, M. Canonical sampling through velocity rescaling. *J. Chem. Phys.* **126**, 014101 (2007).
34. Parrinello, M. & Rahman, A. Polymorphic transitions in single crystals: A new molecular dynamics method. *J. Appl. Phys.* **52**, 7182–7190 (1981).
35. Kumar, S., Rosenberg, J. M., Bouzida, D., Swendsen, R. H. & Kollman, P. A. The weighted histogram analysis method for free-energy calculations on biomolecules. I. The method. *J. Comp. Chem.* **13**, 1011–1021 (1992).
36. Hub, J. S., De Groot, B. L. & Van Der Spoel, D. g_wham: A free weighted histogram analysis implementation including robust error and autocorrelation estimates. *J. Chem. Theory Comput.* **6**, 3713–3720 (2010).
37. Hoffmann, C., Centi, A., Menichetti, R. & Bereau, T. Molecular dynamics trajectories for 630 drug-membrane potentials of mean force. *figshare*. <https://doi.org/10.6084/m9.figshare.c.4641551> (2020).
38. Bereau, T. & Kremer, K. Automated parametrization of the coarse-grained Martini force field for small organic molecules. *J. Chem. Theory Comput.* **11**, 2783–2791 (2015).
39. Monticelli, L. *et al.* The Martini coarse-grained force field: extension to proteins. *J. Chem. Theory Comput.* **4**, 819–834 (2008).
40. Menichetti, R., Kremer, K. & Bereau, T. Efficient potential of mean force calculation from multiscale simulations: solute insertion in a lipid membrane. *Biochem. Biophys. Res. Commun.* **498**, 282–287 (2018).
41. Michaud-Agrawal, N., Denning, E. J., Woolf, T. B. & Beckstein, O. Mdanalysis: a toolkit for the analysis of molecular dynamics simulations. *J. Comp. Chem.* **32**, 2319–2327 (2011).
42. McGibbon, R. T. *et al.* Mdtraj: A modern open library for the analysis of molecular dynamics trajectories. *Biophys. J.* **109**, 1528–1532 (2015).

Acknowledgements

We thank Martin Girard and Omar Valsson for critical reading of the manuscript. This work was supported by the Emmy Noether program of the Deutsche Forschungsgemeinschaft (DFG) and the John von Neumann Institute for Computing (NIC) through access to the supercomputer JURECA at Jülich Supercomputing Centre (JSC).

Author contributions

R.M. designed the methodology. C.H., A.C. and R.M. generated the data. C.H. analyzed the tilt angle. T.B. designed the research. All authors wrote the article.

Competing interests

The authors declare no competing interests.

Additional information

Correspondence and requests for materials should be addressed to T.B.

Reprints and permissions information is available at www.nature.com/reprints.

Publisher's note Springer Nature remains neutral with regard to jurisdictional claims in published maps and institutional affiliations.



Open Access This article is licensed under a Creative Commons Attribution 4.0 International License, which permits use, sharing, adaptation, distribution and reproduction in any medium or format, as long as you give appropriate credit to the original author(s) and the source, provide a link to the Creative Commons license, and indicate if changes were made. The images or other third party material in this article are included in the article's Creative Commons license, unless indicated otherwise in a credit line to the material. If material is not included in the article's Creative Commons license and your intended use is not permitted by statutory regulation or exceeds the permitted use, you will need to obtain permission directly from the copyright holder. To view a copy of this license, visit <http://creativecommons.org/licenses/by/4.0/>.

The Creative Commons Public Domain Dedication waiver <http://creativecommons.org/publicdomain/zero/1.0/> applies to the metadata files associated with this article.

© The Author(s) 2020